Received: 16 September 2020 | Revised: 24 May 2021 | Accepted: 27 May 2021

DOI: 10.1111/jmg.12625

ORIGINAL ARTICLE

Journal of METAMORPHIC GEOLOGY WILEY

# The contribution of elastic geothermobarometry to the debate on HP versus UHP metamorphism

**Mattia Gilio**[1] | **Marco Scambelluri**[2] | **Ross J. Angel**[3] | **Matteo Alvaro**[1]

[1]Department of Earth and Environmental Sciences, University of Pavia, Pavia, Italy

[2]Department of Earth, Environment and Life Sciences, University of Genova, Genova, Italy

[3]IGG-CNR, Padova, Italy

**Correspondence**
Mattia Gilio, Department of Earth and Environmental Sciences, University of Pavia, via Ferrata, 4, Pavia, Italy.
Email: mattia.gilio@unipv.it

**Funding information**
H2020 European Research Council, Grant/Award Number: ERC-STG TRUE DEPTHS - grant agreement 714936

**Handling Editor:** Katy Evans

## Abstract

Characterizing the pressure and temperature (*P–T*) histories of eclogite facies rocks is of key importance for unravelling subduction zone processes at all scales. Accurate *P–T* estimates provide constraints on tectonic and geochemical processes affecting subduction dynamics and help in interpreting the geophysical images of present-day converging plates. Conventional equilibrium geothermobarometers are challenged in ultra high pressure (UHP) metamorphic terranes, as minerals may undergo re-equilibration along their exhumation path. Elastic geobarometry applied to host-inclusion systems is a complementary method to determine *P–T* conditions of metamorphism independent from chemical equilibrium. Because only a single measurement, the inclusion strain, is made, only a line in *P–T* space of possible entrapment conditions, the entrapment isomeke, can be determined. Thus, the entrapment pressure along an isomeke can only be determined if the entrapment temperature is known. An alternative is to calculate entrapment conditions for two types of inclusions that are believed, from petrological evidence such as being in the same garnet growth zone, to have been entrapped at the same time. The intersection between the two sets of isomeke calculated on multiple quartz and zircon inclusions demonstrates that measuring different inclusion phases trapped inside a single host allows unique *P–T* conditions for the host rock to be determined. Here, we combine Zr-in-Rutile thermometry and thermodynamic modelling with micro-Raman measurements on quartz and zircon inclusions trapped in garnet to obtain pressures and temperatures of equilibration of a quartz–garnet vein from the Proterozoic Ulla gneiss basement and of garnet–kyanite gneiss from the Caledonian Blåhø nappe, both in the Fjørtoft UHP terrane, Norway. We find that the quartz–garnet vein formed at high pressure (1.5–2.5 GPa and 750–800°C) and recrystallized at ~1.2 GPa and 880°C. In contrast, the garnet–kyanite gneiss followed an anticlockwise path with peak *P–T* at 1.2 GPa and 880°C: these estimates are consistent with previous thermodynamic modelling and suggest that the Ulla gneiss and the Blåhø nappe came into contact at these last conditions. We also discuss a new method to detect hydrostatic versus Non-hydrostatic stresses near quartz and zircon inclusions in garnet.

**KEYWORDS**

elastic geobarometry, inclusion strain, Raman spectroscopy, Western Gneiss Region

# 1 | INTRODUCTION

Fossil subduction zones provide snapshots of processes and environments that help understanding the evolution of present-day convergent margins (e.g. Stern, 2002). The precise characterization of the *P–T*(t) histories of rocks recording past subduction events is of key importance for having a clearer picture of lithologies and processes occurring at subduction depths (20–80 km), which might ultimately lead to a better understanding of paroxysmal events, like eruptions and earthquakes, affecting the lives of millions of people. An accurate (or inaccurate) *P–T* and/or depth estimate might have important implications for the interpretation of other *P–T*-dependent processes, like subduction-zone fluid geochemistry (e.g. Zheng & Hermann, 2014), element transfer and recycling at volcanic arcs and the seismic imaging interpretation of modern-day subduction zones (e.g. Stern, 2002).

Several UHP terranes worldwide consist of rare pods of UHP rocks within lower pressure lithotypes. The Western Gneiss Region (WGR) in the Scandinavian Caledonites is an example of this structure: UHP conditions are commonly preserved in relatively small pods (from 5 to 150 m to few km wide) of eclogite (e.g. Cuthbert et al., 2000; Terry et al., 2000) and diamond-bearing garnet peridotite/pyroxenite (e.g. van Roermund, 2009; Vrijmoed et al., 2006) embedded within lower grade amphibolite and/or migmatite. In a classic interpretation, this feature is due to the resilience of certain lithologies (i.e. eclogites and garnet peridotites) to maintain, in the absence of hydrous fluid, their UHP mineralogy. Instead, the quartz-rich rocks hosting the eclogitic pods recrystallize more easily at lower pressures during retrogression and water influx, thus pervasively losing evidence of their previous UHP mineralogy. An alternative interpretation was proposed by Vrijmoed et al. (2009), who suggested that the UHP mineral assemblages form in response to a local pressure increase which acted solely on certain lithologies (UHP eclogites and garnet peridotites/pyroxenites), while their host rocks never experienced UHP conditions. This latter interpretation, if confirmed, would significantly change our view of subduction–exhumation processes and the evolution of convergent margins.

In a context where element exchange geothermobarometry (e.g. Krogh Ravna & Terry, 2004; Thomas et al., 2010) and thermodynamic modelling (e.g. Connolly, 1990) are challenged because of re-equilibration issues, elastic thermobarometry can provide a complementary method to unravel *P–T* equilibration conditions. In fact, while being generally well calibrated and consistent within their experimental uncertainties, classical geothermobarometric methods strongly rely on the general assumptions of chemical and thermodynamic equilibrium between the phases under hydrostatic equilibration pressure. Raman thermobarometry is a physics-based method mostly independent of chemical equilibration, potentially able to constrain the *P–T* equilibration conditions (Angel et al., 2019; Rosenfeld & Chase, 1961).

In this study, we performed elastic geothermobarometry on quartz and zircon inclusions trapped in garnet from a quartz–garnet vein and from a garnet–kyanite granulitic gneiss from the Fjørtoft UHP terrane (Norway) and we compared these with results from conventional, chemical-based, geothermobarometry. Here we apply the new elastic thermobarometry method on quartz and zircon inclusions in garnet to eclogite facies rocks where classical element exchange geothermobarometry is challenging, showing how these new results can help to resolve the HP versus UHP conundrum. Furthermore, we bring elastic geobarometry to an even more detailed level, discussing the role of inclusion stress state and pressure recorded by multiple inclusions in a single host.

## 1.1 | Geological background

The WGR of the Scandinavian Caledonides in Norway is the largest exposure of the para-autochthonous basement of the Baltic shield (Corfu et al., 2014). It records a Scandian (430–390 Ma) overprint in amphibolite, granulite, and eclogite facies over Proterozoic (>3.1–1.5 Ga) igneous and metamorphic rocks (Gorbatschev, 1985). The complex metamorphic history of the WGR is currently thought to be the result of multiple burial and exhumation cycles in the period between 450 and 390 Ma (Walczak et al., 2019). Several lenses of HP and UHP eclogite and garnet peridotite occur at different levels of the tectono-stratigraphy (Cuthbert et al., 2000; van Roermund, 2009). Majoritic garnet (van Roermund & Drury, 1998; Scambelluri et al., 2008, 2010) and microdiamonds of Scandian age (Dobrzhinetskaya et al., 1995; van Roermund et al., 2002; Vrijmoed et al., 2006) found within these lenses indicate UHPs, which have been related, assuming lithostatic pressure, to depths exceeding 200 km.

The Fjørtoft island in the Nordøyane archipelago (Norway) hosts one of these UHP lenses (Figure 1a; WGS 84/UTM zone 32V 367320E 6955910N; Robinson et al., 2003). Most of this island consists of a Proterozoic basement of migmatitic gneiss and augen orthogneiss and layered dioritic gneiss with abundant eclogite (the Ulla gneiss) which experienced a Scandian metamorphic overprint at 'normal' HP conditions (700–750°C and ~2.0 GPa; Terry & Robinson, 2003). A strip of Caledonian, diamond-bearing (Dobrzhinetskaya et al., 1995), garnet–kyanite migmatitic paragneiss is exposed in the northern

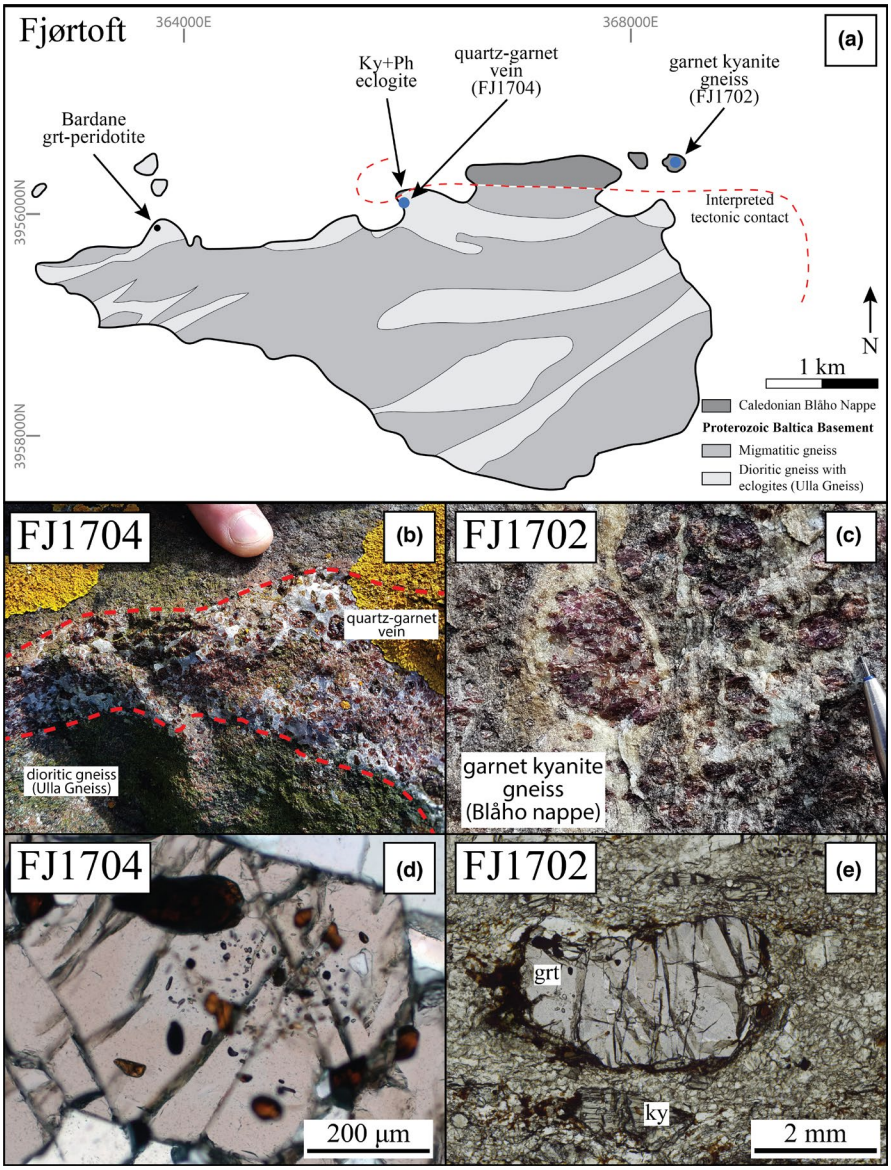


**FIGURE 1** (a) Geological sketch and location of the island of Fjørtoft (modified after Terry et al., 2000). The coordinate system is WGS 84/UTM zone 32V. The blue dots are the sample locations. The dashed red line is the interpreted tectonic contact between the Proterozoic Baltica basement to the south and the Caledonian Blåhø Nappe to the North. The inclusion of the kyanite eclogite within the Caledonian Blåhø Nappe is debated (Carswell et al., 2006; Terry et al., 2000). (b) Field picture of a quartz–garnet vein (Fjørtoft island, Norway). (c) Field picture of a garnet–kyanite gneiss. (d) Parallel-polarized optical micrograph of the quartz–garnet vein (sample FJ1704). Note the inclusion-rich garnet cores and inclusion-poor mantle and rims. (e) Parallel-polarized optical micrograph of the garnet and kyanite porphyroclasts wrapped around a K-feldspar+kyanite+biotite+quartz foliation (sample FJ1702). Mineral abbreviations: Ky, kyanite; Ph, phengite; grt, garnet [Colour figure can be viewed at wileyonlinelibrary.com]

part of the island (Figure 1a). This unit was assigned by Terry et al. (2000) and Terry and Robinson (2003) to the supracrustal Blåhø Nappe, occurring elsewhere on the Nordøyane archipelago and in the nearby islands of Midøy and Otrøy to the South of Fjørtoft. This latter subdivision was proposed to justify the pressure gap between the UHP diamond bearing Blåhø gneiss and the lower pressure Proterozoic Ulla basement. However, some of the eclogite and peridotite pods found within this latter basement display a Scandian UHP metamorphic peak: the Bardane garnet peridotite (1,050°C–6.5 GPa; Scambelluri et al., 2010) and a garnet–kyanite eclogite (Figure 1a; 800°C–4.0 GPa). This latter eclogite pod was originally associated with the Blåhø nappe by Terry et al. (2000), but later repositioned by Carswell and Van Roermund (2005) in the Ulla gneiss, because of the absence of any evident tectonic contact with the Proterozoic basement. However, the relationship between the garnet–kyanite paragneiss of the Blåhø nappe and the structurally lower Ulla gneiss is still debated (Carswell et al., 2006; Walczak et al., 2019).

## 1.2 | Elastic geobarometry of multiple inclusions within a single host

A mineral inclusions can develop residual pressures upon exhumation due to the difference of its thermodynamic properties from those of the surrounding mineral host (Angel et al., 2014; Rosenfeld & Chase, 1961). Consider a soft inclusion in a stiffer host (e.g. quartz in garnet) entrapped at a certain $P$–$T_{HP}$ condition and exhumed to the surface ($P$–$T_0$). At $P$–$T_0$ conditions, both host and inclusion have a larger volume than at entrapment, due to pressure being released upon exhumation ($\Delta V>0$). However, the volume increase in the softer quartz should be greater than that of the stiffer host ($\Delta V_{qz} > \Delta V_{grt}$). The host garnet constrains

the quartz inclusion into a smaller volume than a free quartz crystal, straining, and pressurizing the inclusion. Knowing the inclusion pressure ($P_{inc}$) at room conditions and the thermodynamic properties of host and inclusion allows one to back-calculate a line in *P–T* space of possible entrapment conditions: the isomeke (Angel et al., 2014, 2017; Rosenfeld & Chase, 1961; Tajčmanová et al., 2021). Because only a single measurement, the inclusion strain, is made, only a line in *P–T* space of possible entrapment conditions, the entrapment isomeke, can be determined. Thus, the entrapment pressure along an isomeke can only be determined if the entrapment temperature is known.

Single crystal (e.g. Zr-in-rutile) and element exchange geothermometry (e.g. Fe–Mg content between garnet and pyroxene) are generally reliable methods to constrain the peak equilibration temperature of a rock. However, it is often challenging to couple different methods of geothermobarometry (especially those based on mineral chemistry with those based on mineral physics), as they might indicate different stages, such as mineral growth or re-equilibration, that the rock underwent along its *P–T* path. The Zr-in-rutile thermometer relies on the increase in solubility of zirconia in rutile with temperature in the presence of quartz and zircon (Tomkins et al., 2007; Watson et al., 2006). As the temperature decreases, zirconia is released forming retrograde rims around zircon (Tomkins et al., 2007). However, rutile crystals entrapped in garnet are chemically isolated from quartz and zircons, thus preventing the temperature-driven re-equilibration. As such, we can safely assume that the Zr-in-rutile content of rutile entrapped in garnet indicates the temperature at which the crystal was isolated from the system and that its $ZrO_2$ amount remained unvaried despite changes in pressure and temperature.

An alternative to using Zr-in-rutile geothermometry is to calculate entrapment conditions for two types of inclusions that are believed, from petrological evidence, to have been entrapped at the same time. The bulk modulus of quartz (Angel et al., 2017) is much smaller than that of garnet (Milani et al., 2015), resulting in sub-horizontal isomeke and making quartz an optimal elastic geobarometer. Conversely, the thermal expansion of zircon (~$1.02 \times 10^5$ $K^{-1}$, Ehlers et al., in press) is about half than that of garnet (~$2.54 \times 10^5$ $K^{-1}$, Milani et al., 2015), resulting in high angle isomeke and making zircon an optimal elastic geothermometer. The intersection between the two sets of isomeke calculated on multiple quartz and zircon inclusions demonstrates that measuring different inclusion phases trapped inside a single host allows the determination of unique *P–T* conditions for the host rock. In this study we performed micro-Raman measurements on quartz and zircon inclusions trapped within the same garnet growth zone to obtain a unique point of entrapment in *P–T* space.

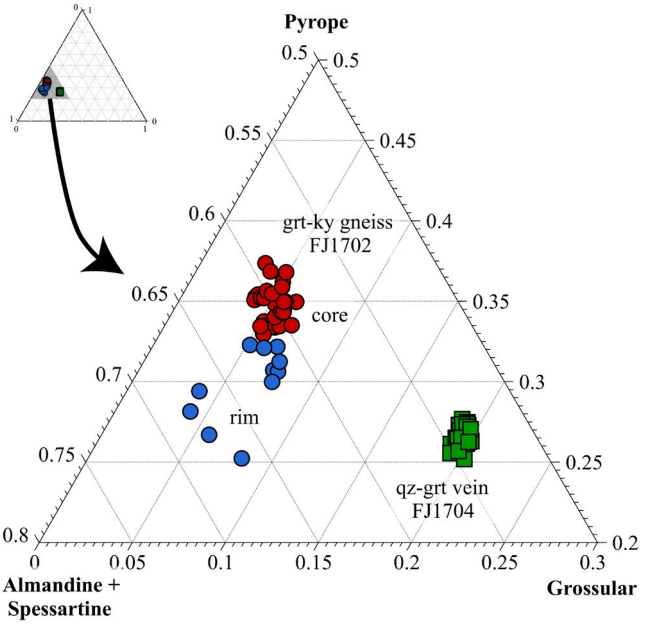


**FIGURE 2** Ternary plot diagram of garnet compositions (grossular, almandine+spessartine and pyrope). Garnet in the quartz–garnet vein (sample FJ1704, green squares) are very homogeneous in composition. Garnet in the garnet–kyanite gneiss (sample FJ1702) display a slight increase in almandine content from core to rim (red and blue circles respectively) [Colour figure can be viewed at wileyonlinelibrary.com]

## 1.3 | Petrography of selected samples

The samples studied (Figure 1a) are a quartz+garnet vein (FJ1704) from the Ulla Gneiss (Terry et al., 2000) and a garnet–kyanite gneiss (FJ1702) from the Blåhø nappe, where microdiamond formation has been documented (Dobrzhinetskaya et al., 1995; Larsen et al., 1998; Liu & Massonne, 2019; Walczak et al., 2019). The vein sample FJ1704 consists of quartz and garnet in equal amounts (Figure 1b,d). Quartz has a granoblastic texture, with intergranular edges connected in triple point junctions, and contains minor inclusions of rutile and apatite (Figure 1d). Garnet is chemically homogeneous (Figure 2; py: 0.27, alm: 0.54, gr: 0.19; repository EMP data) and has inclusion-rich cores and inclusion-poor rims (Figure 1d). Inclusions are rutile and zircon and, in minor amounts, apatite and quartz. While rutile, apatite, and zircon inclusions occur throughout the whole garnet grains, quartz is only at garnet rims. Rutile inclusions range in size from 10 to 20 μm up to 500 μm. Zircon and apatite are generally 30–150 μm long. Quartz inclusions occur as medium-sized (100–300 μm) faceted single crystals. The vein is mostly unaltered, except for minor albite+green amphibole kelyphitic rims replacing garnet around a late vein across the sample.

The Blåhø garnet–kyanite gneiss (sample FJ1702) consists of large (up to 3 cm), first-generation garnet(1) and kyanite(1) porphyroclasts surrounded by a granulitic

foliation of second-generation acicular kyanite(2), K-feldspar, plagioclase, biotite, and quartz (Figure 1c,e). Minor phases include rutile, phlogopite, graphite, and ilmenite. Kyanite(1) is large (up to 5 mm) and consists of variably kinked and deformed porphyroclasts filled with quartz and $N_2$+$CO_2$-bearing fluid inclusions. Garnet is helicitic and contains multiple pre- and syn-growth folded foliations of elongated sillimanite and rare rounded kyanite(2?) in garnet cores (sillimanite pictures and Raman characterization in the Repository), and of kyanite(2) needles in mantles and rims. Furthermore, garnet locally includes kyanite(1) porphyroclasts. Secondary biotite+plagioclase replaces garnet at rims and along fractures (Figure 1e). Rounded quartz, zircon, and apatite crystals occur throughout the garnet. Quartz inclusions are faceted but lacking of any sign of shape maturation such as necking (Cesare et al., 2020). Garnet and some large (>1 mm) quartz grains contain rutile exsolutions and multiple generations of $N_2$+$CO_2$-bearing fluid inclusions (Larsen et al., 1998). Garnet is compositionally zoned and consists of an irregularly shaped core (Figure 2; py: 0.33, alm: 0.60, gr: 0.05, sps: 0.02) and a rim characterized by a decrease in Mg and an increase in Ca (Figure 2; py: 0.27, alm: 0.66, gr: 0.05, sps: 0.02).

## 2 | ANALYTICAL METHODS

We measured the Raman spectra of quartz and zircon inclusions in garnet with a Horiba LabRam HR Evolution spectrometer (holographic gratings of 1,800 grooves/mm) equipped with an Olympus BX41 confocal microscope at controlled temperature of 20(1)°C. The instrument has a spectral resolution of ~2 $cm^{-1}$. Raman spectra were excited using the 532 nm line of a solid-state (YAG) laser. The laser power on the sample surface was ~1–2 mW. The spectrometer was calibrated to the Raman peak of metallic silicon at 520.5 $cm^{-1}$. We used spectra of free crystals with the same composition as the inclusions as further calibrations for the entire spectral range used in our investigation. The collected spectra were baseline corrected for the continuum luminescence background when necessary, temperature reduced to account for the Bose–Einstein occupation factor (Kuzmany, 2009) and normalized to the acquisition time. Peak positions, full widths at half maximum (FWHMs), and integrated intensities were determined from fits with pseudo-Voigt functions. To reduce strain interference due to inclusion proximity to the sample surface, we prepared a section 250 μm thick and we only measured approximately equant inclusions, isolated up to three times their radius, following the approach developed by Zhang (1998), Mazzucchelli et al. (2018) and Campomenosi et al. (2018). For each of the selected Raman bands we determined the change in peak position $\Delta\omega$ of the Raman band as the difference between the Raman shift of the inclusion $\omega_i$ from that of an unstrained reference crystal ($\omega_0$). As standards, we used free (unstrained) quartz (mineralogical collection uniPV) and zircon (Mud Tank Hill, Australia) crystals, measured multiple times during each measurement session at ambient pressure and temperature (0.1 MPa and 20°C) to eliminate shifts in peak positions due to instrumental drift and/or minor changes in room temperature. The $\omega_0$ values were averaged and then subtracted from the $\omega_i$ of the strained inclusions analysed in between two consecutive standard measurements. For zircon inclusions, because of the possible misinterpretations due to effects of radiation damage (e.g. which shifts the Raman peaks and changes significantly the elastic properties of zircon; Binvignat et al., 2018) we adopted the procedure described in Campomenosi et al. (2020). Therefore, we included in the analysis only inclusions with a FWHM of the Raman peak near 1,014/1,008 $cm^{-1}$ < 5 $cm^{-1}$ (radiation damage threshold; see Campomenosi et al., 2020). Unfortunately, Raman spectra from all the measured zircons in sample FJ1702 (garnet–kyanite gneiss) exceeded this threshold and give inclusion pressures $P_{inc}$ > 1 GPa. These values of $P_{inc}$ give unrealistic entrapment temperatures (>1,000°C at 1.0 GPa for the case of zircon in pyrope) and were therefore discarded as being an effect of the radiation damage. The $\Delta\omega$ values of each mode of zircon and quartz inclusions and unstrained standards are listed in the repository database. Finally, sets of $\Delta\omega$ for each inclusion (modes $\omega_{128}$, $\omega_{206}$, $\omega_{265}$, and $\omega_{464}$ for quartz and modes $\omega_{197}$, $\omega_{214}$, $\omega_{223}$, $\omega_{342}$, $\omega_{438}$, $\omega_{969}$, and $\omega_{1014}$ for zircon, as they are generally unaffected by overlap with modes of the host garnet) have been used to determine strain using the software stRAinMAN (Angel et al., 2019) by employing the Grüneisen tensors for quartz (Murri et al., 2018) and zircon (Stangarone et al., 2019).

In-situ major element ($SiO_2$, $TiO_2$, $Al_2O_3$, $Cr_2O_3$, FeO, MgO, MnO, CaO, NiO, $Na_2O$, and $K_2O$) compositions of minerals were measured using a JEOL JXA 8200 Superprobe equipped with five wavelength dispersive spectrometers (WDSs), an energy dispersive spectrometer, and a cathodoluminescence detector (accelerating potential 15 kV, beam current 15 nA), operating at the Dipartimento di Scienze della Terra, University of Milano. The measurements of all elements were performed with a counting time of 30 s. Zirconium in rutile was analysed using the same WDS instrument, set with an accelerating potential of 15 kV and a beam current of 97.6 nA. The WDS signal of Ti was used as fixed standard mass to estimate the Zr content.

# 3 | RESULTS

## 3.1 | Temperature estimates: Zirconium-in-rutile

Rutile inclusions in garnet from both samples were measured for their Zr content to apply Zr-in-rutile geothermometry. The rutile identified using backscattered electron imaging showed no obvious growth patterns. Temperature was estimated with the Watson et al. (2006), Tomkins et al. (2007) and Kohn (2020) calibrations. At 1.0 GPa, the difference in temperature given by the three calibrations is ≤10°C (Table 1). However, in the following we will use solely the new calibration by Kohn (2020) in order to have a greater accuracy at high pressures. In the vein sample FJ1704, results from Zr-in-rutile thermometry are consistent within uncertainties, giving an average temperature of 705 ± 10°C at 1.0 GPa and 760 ± 10°C at 2.0 GPa. In the gneiss sample FJ1702, two distinct temperature groups were observed: rutile in garnet cores and mantles give an average $T = 823 \pm 30$°C and those in the garnet rims $T = 737 \pm 15$°C, both calculated at $P = 1.0$ GPa.

## 3.2 | Residual strain estimates and residual pressure determination

Results from Raman measurements on zircon and quartz inclusions from sample FJ1704 (quartz–garnet vein) and FJ1702 (garnet–kyanite gneiss) are shown in Figures 3 and 4 and reported in the repository datafile. The strain state of quartz and zircon inclusions, together with their 2σ confidence ellipses is displayed in Figure 3a,b. The strain of each inclusion was converted to stress using the elastic tensors at room *P–T* for quartz (Wang et al., 2015) and zircon (Özkan et al., 1974). The $P_{inc}$ (Figure 3c,d) was calculated from the stress tensor as the negative of the mean normal stress ($P_{inc} = -\frac{\sigma_1+\sigma_2+\sigma_3}{3}$). To avoid the effects of strain localization at corners and inclusion shape effects (Campomenosi et al., 2020; Mazzucchelli et al., 2018), each Raman measurement was performed at the center of well-rounded quartz and zircon inclusions.

Garnet in both samples (FJ1702 and FJ1704) is rather homogenous in composition making it hard to distinguish between core, mantle, and rim by the major element chemistry. In sample FJ1704, the garnet cores have a very high density of tiny rutile inclusions, while garnet rims are inclusion poor. In sample FJ1702, garnet zone boundaries were defined by sharp changes in $P_{inc}$ (Figure 3).

## 3.3 | Raman geobarometry on quartz and zircon

The $P_{inc}$ of quartz inclusions is the same, within a 2σ uncertainty, for inclusions within the same garnet growth zone (i.e. core, mantle, and rim). The same is true for the zircon inclusions. Therefore, we averaged the $P_{inc}$ of the same inclusions from the same growth zone (least-squares weighted average) to calculate an entrapment isomeke representative of each zone. The entrapment isomekes for quartz and zircon inclusions in samples FJ1704 and FJ1702 (Figure 4a,b) were obtained from the $P_{inc}$ with the EoSfit–Pinc software (Angel, Mazzucchelli, et al., 2017) and the EntraPT software by (Mazzucchelli et al., 2021), using the equation of state of quartz (Angel, Alvaro, et al., 2017), zircon (Ehlers et al., in press) and, in the absence of reliable EoS for garnet solid solutions, pure pyrope (Milani et al., 2015). Using an almandine EoS leads to entrapment pressures systematically 0.10–0.17 GPa higher than those quoted here, but the pattern of pressures is maintained, so it is likely that an appropriate EoS for these garnet compositions will raise the calculated entrapment pressures by less than 0.1 GPa. The average $P_{inc}$ for core zircons (thick red line in Figure 4a) and Zr-in-rutile thermometry (orange field) suggests garnet cores formed in the *P–T* range of 720–800°C and 1.5–2. GPa. The entrapment isomekes of rim quartz and zircon cross at *P–T* of 870–890°C and 1.3–1.4 GPa. Pressure–temperature estimates for both garnet cores and rims fall within the field of garnet+quartz stability constrained by thermodynamic modelling in the simple KFMASH system (greyish area in Figure 5). This latter was calculated using PerpleX (Connolly, 1990) with the thermodynamic database hp11ver.dat (Holland & Powell, 2011; https://www.perplex.ethz.ch) and the solution models described in Powell et al. (1998). In sample FJ1702 (Figure 4b), the entrapment isomeke for quartz in garnet core (red line) crosses the *P–T* area suggested by Liu and Massonne (2019) for the growth of garnet cores at $T \sim 880$C and $P \sim 1.2$ GPa. The average isomeke for quartz inclusions in mantle and rim, with Zr-in-rutile temperature estimates for the same garnet growth zones, suggests *P–T* conditions of entrapment of 800–850°C–1.1 GPa for garnet mantle and of 700–750°C–1.0 GPa for garnet rim (Figure 4b).

# 4 | DISCUSSION AND IMPLICATIONS

## 4.1 | Isotropic approximation for quartz and zircon

Raman spectroscopy has been extensively used to measure $P_{inc}$ of inclusions (e.g. Kohn, 2014; Thomas & Spear, 2018).

**TABLE 1** Zircon-in-rutile (ppm) and temperature estimates using calibrations by Tomkins et al. (2007)[1], Watson et al. (2006)[2] and Kohn (2020)[3] at $P = 1.0$ GPa

| Sample | Analysis | | $ZrO_2$ (wt%) | Zr (ppm) | d.l. (ppm) | $T^1$ (°C) | $T^2$ (°C) | $T^3$ (°C) | 2σ |
|---|---|---|---|---|---|---|---|---|---|
| FJ1702 | Rt_01 | Rim | 0.1231 | 911.3 | 45 | 749 | 743 | 741 | 36 |
| FJ1702 | Rt_02 | Rim | 0.09 | 666.3 | 46 | 719 | 712 | 709 | 35 |
| FJ1702 | Rt_03 | Rim | 0.1728 | 1,279.3 | 45 | 783 | 778 | 775 | 38 |
| FJ1702 | Rt_04 | Rim | 0.1085 | 803.2 | 45 | 736 | 730 | 728 | 36 |
| FJ1702 | Rt_05 | Rim | 0.1175 | 869.9 | 46 | 744 | 738 | 736 | 36 |
| FJ1702 | Rt_06 | Mantle | 0.262 | 1,939.6 | 45 | 829 | 825 | 819 | 40 |
| FJ1702 | Rt_07 | Rim | 0.1218 | 901.7 | 44 | 748 | 742 | 740 | 36 |
| FJ1702 | Rt_08 | Mantle | 0.2542 | 1,881.9 | 46 | 826 | 821 | 815 | 40 |
| FJ1702 | Rt_09 | Rim | 0.1095 | 810.6 | 45 | 737 | 731 | 729 | 36 |
| FJ1702 | Rt_10 | Rim | 0.1058 | 783.2 | 46 | 734 | 728 | 725 | 35 |
| FJ1704 | Grt_01_Rt_01 | | 0.0707 | 523.4 | 46 | 697 | 690 | 686 | 34 |
| FJ1704 | Grt_01_Rt_02 | | 0.0837 | 619.6 | 45 | 712 | 705 | 702 | 35 |
| FJ1704 | Grt_01_Rt_03 | | 0.0789 | 584.1 | 46 | 707 | 700 | 697 | 34 |
| FJ1704 | Grt_01_Rt_04 | | 0.0781 | 578.2 | 45 | 706 | 699 | 696 | 34 |
| FJ1704 | Grt_01_Rt_05 | | 0.0746 | 552.3 | 45 | 702 | 695 | 691 | 34 |
| FJ1704 | Grt_01_Rt_06 | | 0.0721 | 533.8 | 46 | 698 | 692 | 688 | 34 |
| FJ1704 | Grt_01_Rt_07 | | 0.0819 | 606.3 | 46 | 710 | 703 | 700 | 35 |
| FJ1704 | Grt_01_Rt_08 | | 0.0745 | 551.5 | 46 | 701 | 695 | 691 | 34 |
| FJ1704 | Grt_01_Rt_09 | | 0.0749 | 554.5 | 46 | 702 | 695 | 692 | 34 |
| FJ1704 | Grt_01_Rt_10 | | 0.0813 | 601.9 | 45 | 709 | 703 | 700 | 34 |
| FJ1704 | Grt_01_Rt_11 | | 0.0797 | 590 | 46 | 707 | 701 | 698 | 34 |
| FJ1704 | Grt_01_Rt_12 | | 0.0826 | 611.5 | 45 | 711 | 704 | 701 | 35 |
| FJ1704 | Grt_02_Rt_01 | | 0.0829 | 613.7 | 45 | 711 | 705 | 701 | 35 |
| FJ1704 | Grt_02_Rt_02 | | 0.0732 | 541.9 | 45 | 700 | 693 | 689 | 34 |
| FJ1704 | Grt_02_Rt_03 | | 0.0778 | 576 | 45 | 705 | 699 | 695 | 34 |
| FJ1704 | Grt_02_Rt_04 | | 0.0804 | 595.2 | 45 | 708 | 702 | 699 | 34 |
| FJ1704 | Grt_02_Rt_05 | | 0.0754 | 558.2 | 45 | 702 | 696 | 692 | 34 |
| FJ1704 | Grt_02_Rt_06 | | 0.0877 | 649.3 | 46 | 716 | 710 | 707 | 35 |
| FJ1704 | Grt_02_Rt_07 | | 0.0757 | 560.4 | 46 | 703 | 696 | 693 | 34 |
| FJ1704 | Grt_02_Rt_08 | | 0.0727 | 538.2 | 45 | 699 | 692 | 689 | 34 |
| FJ1704 | Grt_02_Rt_09 | | 0.0757 | 560.4 | 45 | 703 | 696 | 693 | 34 |
| FJ1704 | Grt_02_Rt_12 | | 0.0594 | 439.7 | 44 | 681 | 675 | 670 | 34 |
| FJ1704 | Grt_02_Rt_13 | | 0.0782 | 578.9 | 46 | 706 | 699 | 696 | 34 |
| FJ1704 | Grt_02_Rt_16 | | 0.0808 | 598.2 | 45 | 709 | 702 | 699 | 34 |
| FJ1704 | Grt_02_Rt_17 | | 0.0895 | 662.6 | 45 | 718 | 712 | 709 | 35 |

These methods, which rely on the direct correlation of Raman shifts of a single mode with hydrostatic pressure, are essentially incorrect, as the mode shift from reference position in a crystal is strain- rather than pressure dependent (e.g. Angel et al., 2019; Gilio et al., in press). Once the inclusion strain is measured, two approaches are possible to recalculate the *P–T* conditions of entrapment: the isotropic and anisotropic approximation. In the isotropic approximation (Angel et al., 2014), an isomeke is calculated from each inclusion $P_{inc}$, giving a line of possible entrapment conditions in the *P–T* space. Here we show that, by crossing the volume isomekes of two different mineral inclusions (e.g. quartz and zircon) likely entrapped at the same time, we obtain a single point in the *P–T* space (FJ1704 rim in Figure 4a). In the anisotropic approximation (Alvaro et al., 2020), the two crossing lines are given by the evolution of the *a*- and *c*-axis of quartz in *P–T* space that are considered separately to calculate lines of possible entrapment

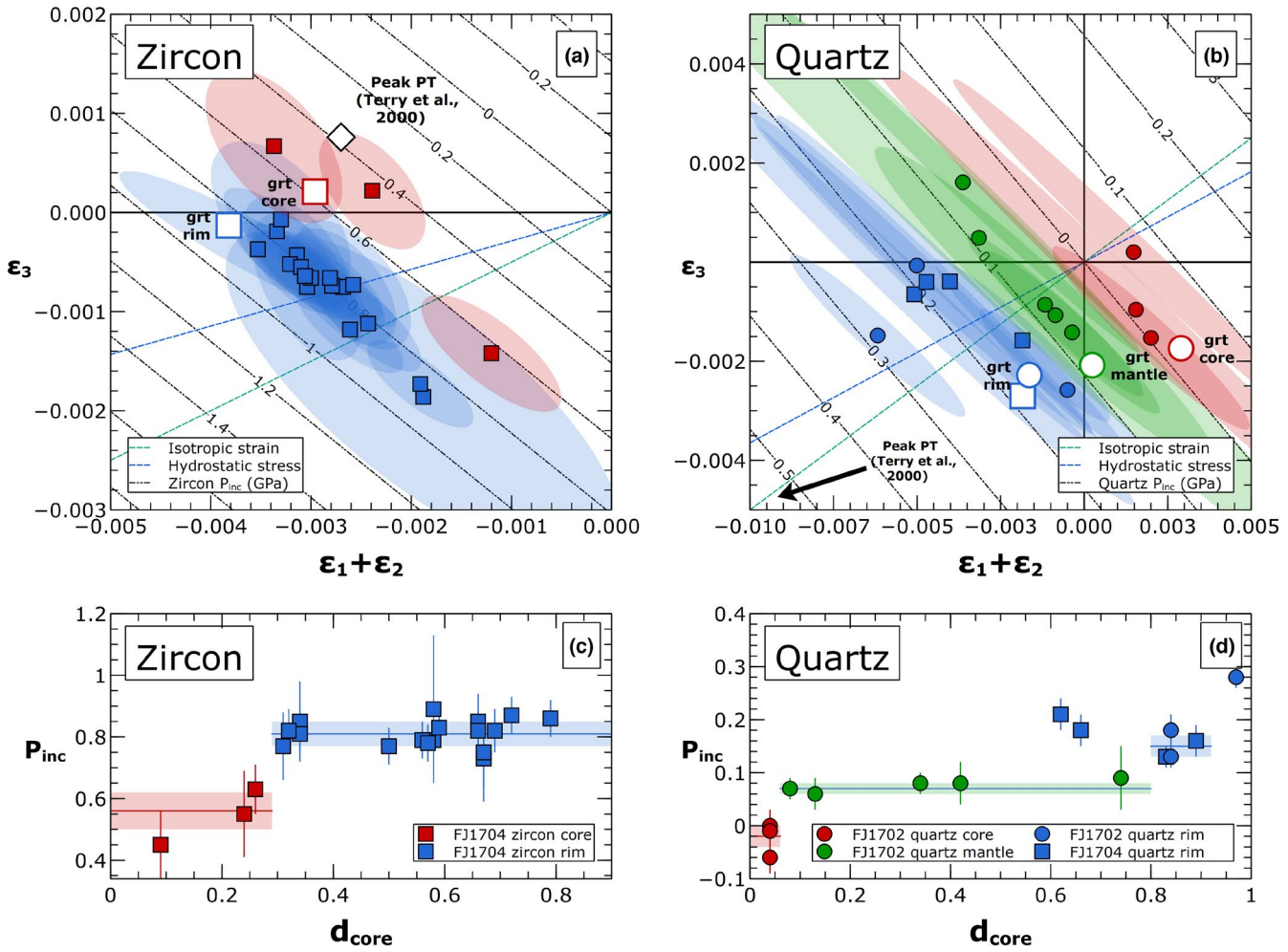


**FIGURE 3** Strains and $P_{inc}$ versus normalized distance of zircon (a and c) and quartz (b and d) inclusions in garnet from the quartz–garnet veins (FJ1704; square symbols) and the garnet–kyanite gneiss (FJ1702; circle symbols). The symbol colour indicates the occurrence of such inclusions within garnet cores (red), mantles (green; only in b), and rims (blue). The strain diagrams (a and b) also include the lines of equal $P_{inc}$, of isotropic strain and of hydrostatic stress (i.e. the Reuss and Voigt boundaries) for zircon (a) and quartz (b). In (a) and (b), the large open symbols with red, green (only in b), and blue outer margins are the strain states expected for zircons (squares) and quartz (circles) entrapped at the *P–T* conditions found by crossing quartz and zircon isomeke and with Zr-in-rutile thermometry (see Figure 4). The white diamond symbol represents the strain state that a zircon would have if entrapped at peak *P–T* conditions (4.0 GPa—800°C, Terry et al., 2000). Note that the expected strain for quartz entrapped at peak condition ($\varepsilon_1 + \varepsilon_2 = -0.029$; $\varepsilon_3 = -0.011$; $P_{inc} = 1.5$ GPa) plots out of the chart. These strains were calculated following the method described in Alvaro et al. (2020), using the axial equations of states of quartz (Angel, Alvaro, et al., 2017) and zircon (Ehlers et al., in press). The shaded areas in (c) and (d) are the inverse variance weighted average and uncertainty of the $P_{inc}$ for core (red), mantle (green, only in d), and rim (blue) [Colour figure can be viewed at wileyonlinelibrary.com]

conditions for each unit cell axis (we refer to these as lattice isomekes). The intersection of these two lines provides a unique point of entrapment in the *P–T* space for each inclusion. Although appealing, using lattice isomekes requires a very precise determination (uncertainty $<10^{-4}$) of the strain state of the inclusion at room *P–T*. These levels of precision can be reached only by measuring the lattice parameter of the inclusion via single crystal X-ray diffraction, while the uncertainty on strain from Raman spectroscopy is commonly ~0.001–0.003 due to the strong covariance of $\varepsilon_1+\varepsilon_2$ and $\varepsilon_3$. This is because most Raman lines of quartz and zircon have similar ratios of Grüneisen tensor components $\gamma_1/\gamma_3$, so the isoshift lines in strain space cross at low angles and their point of intersection is not well constrained. This strong negative covariance means that volume strain is better constrained than the individual strain values by Raman measurements, and that the confidence ellipses from such measurements are generally very elongate. The 2σ confidence ellipses (Figure 3) have their major axes approximately parallel to the lines of equal $P_{inc}$. As such, the uncertainty on the $P_{inc}$ is generally much smaller than that of the axial strains, which means that the isotropic approximation may be more reliable than the anisotropic analysis for strains measured with Raman spectroscopy.

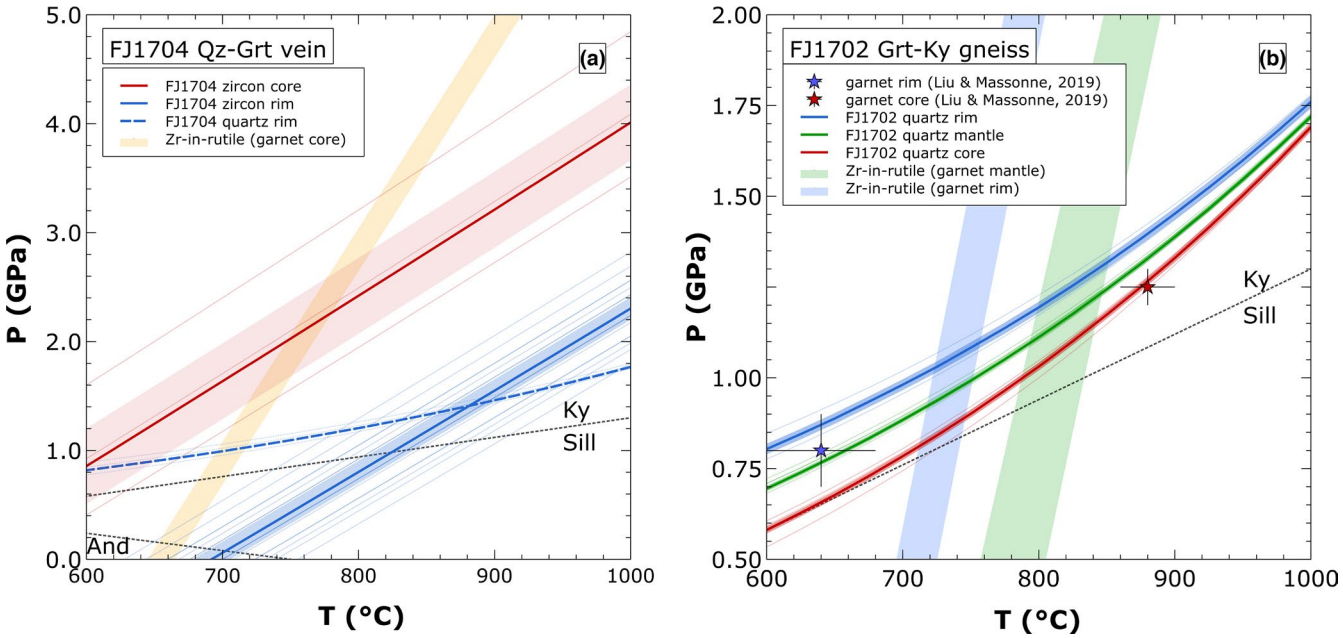


**FIGURE 4** Isomeke of zircon and quartz in garnet from the quartz–garnet vein (FJ1704; a) and the garnet–kyanite gneiss (FJ1702; b). The thin lines are the entrapment isomekes of single inclusions while the thick lines and their associated shaded areas are the entrapment isomekes for the averaged $P_{inc}$ showed in Figure 3c,d. The red and blue star symbols in (b) are the *P–T* estimates by Liu and Massonne (2019) for garnet cores and rims, respectively, obtained with classical geothermobarometric methods and thermodynamic modelling. The difference in slope between the entrapment isomekes of zircon and quartz is due to their difference in thermal expansion and bulk modulus. The intercept between zircon and quartz entrapment isomekes of inclusions within the same garnet zone makes an optimal geothermobarometer. In garnet cores from sample FJ1704 (a), quartz inclusions were absent and the entrapment isomekes for zircons were crossed with the temperature estimates from Zr-in-rutile thermometry (orange shaded area). Similarly, in sample FJ1702 (b), zircons had a too extensive radiation damage to be usable for elastic geobarometry. In this latter case, the entrapment isomekes for quartz inclusions in mantles and rims were crossed with the temperature estimates from rutile in the same growth zone of garnet (green shaded area for garnet mantles and blue for rims). No rutile was found at garnet cores; nonetheless the entrapment isomekes for quartz at garnet cores is consistent with *P–T* estimates from Liu and Massonne (2019) for the same garnet growth zone [Colour figure can be viewed at wileyonlinelibrary.com]

### 4.1.1 | *P–T* evolution

Petrology and microstructure of the Ulla quartz–garnet vein (FJ1704) suggest that inclusion-rich garnet cores and inclusion-poor rims formed at two distinct stages along the *P–T* history of the vein. This multistage evolution is consistent with a difference in *P–T* trapping conditions recorded by the zircons at the garnet core (higher pressure) and by those at the garnet rim (lower pressure, Figure 4). The pressure conditions achieved by the intersection of the core zircon isomeke and the Zr-in-rutile isopleths (720–800°C–1.5–2.5 GPa) are significantly lower than the peak UHP (800°C–4.0 GPa) suggested for the nearby Ulla kyanite–eclogite body by Terry et al. (2000). Our pressure estimate is, however, only a mean normal stress, as the inclusion stresses are generally in the form $\sigma_1 = \sigma_2 \neq \sigma_3$. As such, the quartz–garnet vein might have formed in a pressure range from 1.5 to 3.0 GPa under variable differential stress, while the rims formed at lower pressure (Figure 5). The isomeke of quartz and zircon inclusions at garnet rims intersects at 820–880°C and 1.2–1.4 GPa, giving a precise *P–T* estimate for the crystallization or re-equilibration of the vein. Nevertheless, the effects of temperature-driven post-entrapment reset of the zircon- and quartz-in-garnet inclusion pressure (Campomenosi et al., 2021), as well as the uncertainty introduced by using a pure end-member EoS in the calculation are still unclear. This might result in an underestimation of the uncertainty of the final pressure and temperature of entrapment.

In the garnet–kyanite Blåhø gneiss (FJ1702), calculated *P–T* crystallization conditions for garnet cores from both quartz-in-garnet elastic barometry and thermodynamic modelling are consistent at 880°C and 1.2 GPa. Garnet mantles and rims grew during an almost isobaric cooling down to *P–T* as low as 640°C and 0.8 GPa (Liu & Massonne, 2019), within the kyanite stability field. One of the main issues in the *P–T* evolution of the Blåhø gneiss regards the finding of metamorphic microdiamonds (Dobrzhinetskaya et al., 1995), suggesting a UHPM origin of the garnet+kyanite mineral assemblage. However, the recent paper by Liu and Massonne (2019) questions the validity of such an interpretation and, based on *P–T* pseudosection modelling, provides an alternative evolution of this terrane that suggests peak metamorphic conditions at 1.2 GPa a ~880°C. Our elastic thermobarometric estimates for the Blåhø nappe peak *P–T* coincide with the

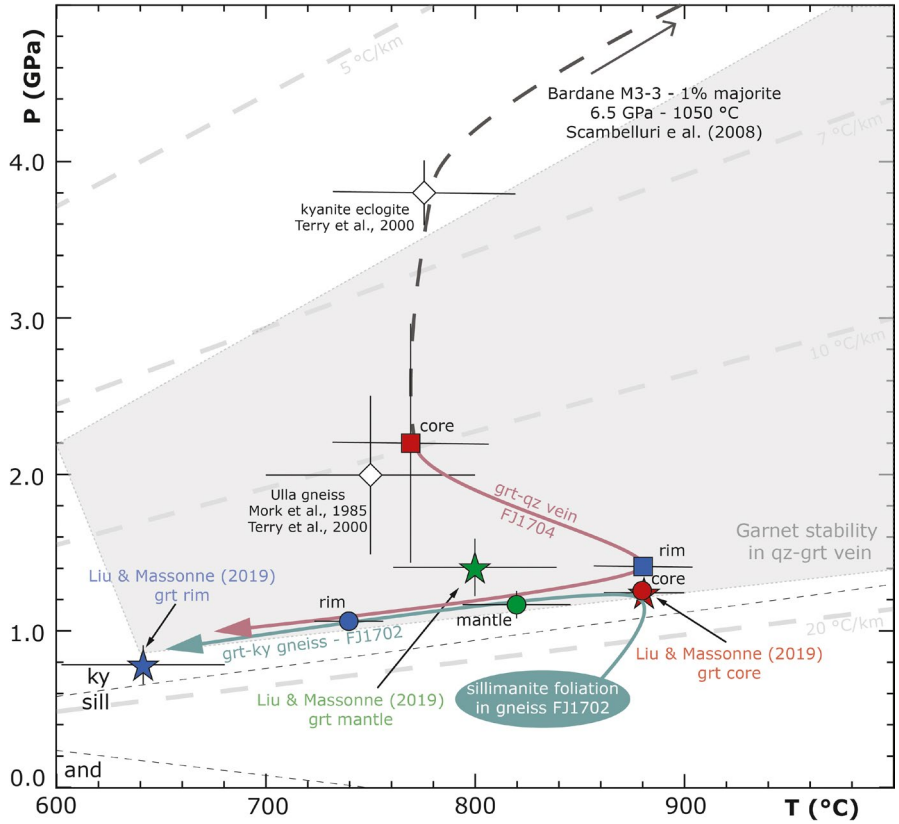


**FIGURE 5** Pressure–temperature (*P–T*) of the quartz–garnet veins (red arrow), the garnet–kyanite gneiss (green arrow). The symbols indicate *P–T* estimates for garnet core (red), mantle (green; only the gneiss) and rim (blue). The grey dashed *P–T* path is the retrograde path from UHP conditions inferred for the Ulla gneiss, assuming the kyanite eclogite described in Terry et al. (2000) belongs to the Ulla gneiss. The large grey shaded area is the stability field of garnet in the quartz–garnet vein obtained from thermodynamic modelling, with the constant composition shown in Figure 2. The red, green and blue star symbols are the *P–T* estimates for garnet core, mantle and rim in the garnet–kyanite gneiss proposed by Liu and Massonne (2019). The figure also includes the *P–T* estimates for the kyanite eclogite (Terry et al., 2000) and for other eclogite pods in the Ulla gneiss (Mørk, 1985; Terry et al., 2000), the andalusite (and), sillimanite (sill) and kyanite (ky) stability reaction lines (thin dashed grey lines), and the geothermal gradients for 5, 7, 10 and 20°C/km, assuming hydrostatic pressure (think dashed grey lines). The *P–T* conditions for the M3-–3 majoritic garnet in Bardane (Ulla Gneiss; 6.5 GPa–1,050°C; Scambelluri et al., 2008) plot outside the area of this figure [Colour figure can be viewed at wileyonlinelibrary.com]

ultra high temperature ones from the thermodynamic modelling (Liu & Massonne, 2019). Moreover, we document the presence of a relict sillimanite foliation with small kyanite crystals at garnet cores (Repository data set), indicating that the rock reached peak *P–T* conditions in the granulite facies along an anticlockwise *P–T* path starting from lower pressures in the sillimanite stability field, and not along a retrograde path from UHPM conditions (Figure 5).

Faceted quartz inclusions in garnet may indicate post-entrapment shape change, which might lead to a reset of the elastic strain of the inclusions (Cesare et al., 2020). In the absence of plastic deformation of the host garnet, differences in *P–T*–t and stresses do not affect the results, as the strain measured by Raman spectroscopy is purely elastic (and thus reversible). In turn, plastic deformation in garnet might reset the inclusion pressure, leading to two possible outcomes. (a) In case of a complete reset, all inclusions within a garnet will have the same strain within uncertainty and the measured strain would correspond to the point in *P–T* space where the garnet behaviour reverted from plastic to elastic, for example on cooling. (b) Instead, a partial reset would result in a set of widely scattered calculated strains with values between those expected for entrapment at the original entrapment *P–T* and the re-equilibration conditions. The residual pressure of quartz and zircon inclusions measured in sample FJ1702 and FJ1704 is directly correlated with the distance of each inclusion from the garnet core (Figure 3). The residual pressures remain constant within the same garnet growth zone and change from one zone to another. The observed patterns of inclusion pressures therefore indicate that it is unlikely that the measured inclusions underwent post-entrapment re-equilibration.

The new *P–T* estimates presented here confirm the complexity of the metamorphic evolution experienced by the rocks in the island of Fjørtoft (Walczak et al., 2019). The garnet–kyanite gneiss presented here lacks major mineralogical evidence for an UHP equilibration before its current,

lower pressure, mineral assemblage. The microdiamonds, (Dobrzhinetskaya et al., 1995) hinting of such an UHP event, might be the sole remnants of a previous UHP mineral assemblage, completely erased by lower pressure recrystallization in the amphibolite and granulite facies or, as alternatively suggested by Liu and Massonne (2019), the result of saw contamination or of the presence of detrital diamonds. Conversely, rutile exsolution needles in garnet and quartz, commonly found in high-grade granulites (Ague & Eckert, 2012; Liu & Massonne, 2019), suggest the garnet was equilibrated at very high temperatures. The Ulla quartz–garnet vein records HP conditions of formation which denote a sharp pressure gap with its host rock (lower pressure amphibolitic ortho-derivates of the Ulla gneiss) and a recrystallization stage (garnet rims) at low-*P* and UHT conditions like those experienced by the garnet–kyanite gneiss of the Blåhø nappe during growth of garnet cores. In this scenario (Figure 5), the Ulla gneiss might have experienced an early subduction stage to UHP conditions (up to 6.5 GPa and 1,000°C; Scambelluri et al., 2008) followed by exhumation and concurrent cooling down to 2.0–4.0 GPa and 750–800°C, where most eclogites in the area re-equilibrated and where the garnet–kyanite vein formed. Terry et al. (2000) performed detailed mapping and structural analysis of the Nordøyane archipelago and concluded that the Blåhø nappe and the Ulla gneiss came into contact at HT and $P \sim 1.1$–$1.8$ GPa during the retrograde path from UHP. The Ulla gneiss was then heated to temperatures of ~880°C at 1.2 GPa, probably because of the different geotherm at lower pressure and the contact with the HT Blåhø nappe (red and green *P*–*T* paths in Figure 5). After that, the two units (Ulla gneiss and Blåhø nappe) followed a near-isobaric cooling to 0.8 GPa and 650°C, to be then exposed to the surface.

This late-stage heating event, shared by both the Ulla gneiss and the Blåhø nappe, is probably responsible for the migmatization of most hydrated granitic and quartzofeldspathic rocks in the area. Drier and silica-poor lithologies such as garnet peridotites and anhydrous eclogites might have escaped migmatization due to their higher melting points and they still preserve the original high-*P* to UHP mineral assemblages. Furthermore, the garnet–kyanite vein in the Ulla gneiss records both the high-*P* and the high-*T* stage. This seems to exclude, at least in the case of the island of Fjørtoft, that the UHP was confined to local pressure increases due to non-lithostatic stresses and/or partial melting (Vrijmoed et al., 2009), but it was experienced by the whole tectonic unit, instead.

### 4.1.2 | Raman spectroscopy and inclusion strain

Raman geobarometry allows the measurement of the strain state of inclusions, considered as single $\varepsilon_1$, $\varepsilon_2$, and $\varepsilon_3$ components. This allows the changes in Raman shift to be interpreted in terms of stress acting at entrapment in the immediate environment of the inclusions. As such, we can use elastic anisotropy to investigate palaeo-stresses and their evolution over time, challenging one of the major assumptions in the application of solid-state thermodynamics to mineral equilibria: considering stress to be always hydrostatic.

Using the concept of axial isomekes (Alvaro et al., 2020), coupled with the numerical solutions by Mazzucchelli et al. (2019), we calculated the expected strain state for an inclusion entrapped at the *P*–*T* conditions corresponding to our estimates for garnet cores, mantles, and rims (red, green, and blue symbols in Figure 3a,b, respectively) and for the peak *P*–*T* condition of the area (4.0 GPa and 820°C; Terry et al., 2000; Figure 3; the strains expected in quartz for such *P*–*T* conditions are $\varepsilon_1 + \varepsilon_2 = -0.029$; $\varepsilon_3 = -0.011$ and fall outside the chart limits). To calculate these strains, we assumed that quartz and zircon were entrapped under hydrostatic stress and exhumed back to the surface with no perturbations of their elastic response (e.g. plastic deformation). In the quartz–garnet vein (FJ1704), the strains calculated for the garnet rim inclusions (blue empty square symbol) fall within the 2σ confidence ellipsoid of most zircons (Figure 3a). This suggests that such inclusions were trapped under hydrostatic stress conditions, assuming all inclusions are randomly oriented. The same behaviour is observed in all quartz inclusions, in both samples (Figure 3b). Instead, zircon inclusions in the core of garnet from sample FJ1704 (red symbols in Figure 3a) show a different behaviour. The strain state of two inclusions, considering their confidence ellipses, barely overlaps with the strains expected for garnet core inclusions (red empty square). However, a third inclusion, despite having similar $P_{inc}$ to the other two, has a significantly different strain state.

One possible way to explain this strain distribution is to consider a set of randomly oriented inclusions entrapped in garnet (cubic and nearly elastically isotropic) under a non-hydrostatic stress field. In fact, regardless of their orientations, inclusions entrapped in a cubic host under a hydrostatic stress field, will deform isotropically. This is because the host garnet always imposes an isotropic strain on the inclusion: the space that garnet allocates for the inclusion changes in dimensions with pressure and temperature, but its shape remains unchanged. Conversely, an inclusion entrapped in a cubic garnet under a non-hydrostatic stress field, will be subject to strains depending on the external stress field, on the elastic properties of the host and on the inclusion orientation with respect to the stress field (Mazzucchelli et al., 2019). The strain distribution of zircon inclusions in the core of garnet from sample FJ1704 (Figure 3a) suggests they were entrapped under non-hydrostatic conditions. Regardless the values of the independent strain components, to a first approximation the volume strain ($\varepsilon_1 + \varepsilon_2 + \varepsilon_3$) of such randomly oriented

crystals will be similar, and thus will give roughly the same $P_{inc}$ (Figure 3c,d). For this reason, the isotropic method of calculating the isomeke (Angel, Mazzucchelli, et al., 2017) remains valid, even though giving constraints only on the mean normal stress acting on inclusions entrapped under a non-hydrostatic stress. Thus, measuring inclusion strains allows one to qualitatively estimate whether, at entrapment and around the inclusion, the local stress state was hydrostatic or non-hydrostatic, despite being unable to quantify the actual differential stresses.

## 5 | CONCLUSIONS

1. Elastic geothermobarometry applied to quartz and zircon inclusions in garnet is a fast and reliable method to obtain estimates on equilibration pressure and temperature in metamorphic rocks. Quartz and zircon isomekes can be used as a geobarometer and geothermometer respectively and together provide a unique point in *P–T* space, assuming the two phases were entrapped synchronously. This method is especially useful in rock types where classical geothermobarometry is challenging, like the quartz–garnet vein (sample FJ1704).
2. Individual axial inclusion strains determined by Raman spectroscopy have rather large uncertainties, making the anisotropic approach of elastic geothermobarometry unfeasible. However, the uncertainty in volume strain is much smaller, allowing a good determination of the entrapment isomeke using the isotropic approximation.
3. Our study shows that the quartz–garnet vein from the Proterozoic Ulla gneiss basements formed at high pressure (1.5–2.5 GPa and 750–800°C) and recrystallized at ~1.2 GPa and 880°C. Instead, the garnet–kyanite gneiss from the Caledonian Blåhø nappe followed an anticlockwise path with peak *P–T* at 1.2 GPa and 880°C, consistent with previous thermodynamic modelling, where it coupled with the UHP Ulla gneiss.
4. Measuring inclusion strains allows qualitative estimates of whether the stress around the inclusions, at entrapment, was hydrostatic or non-hydrostatic.

## ACKNOWLEDGEMENTS

This project received funding from the European Research Council under the European Union's Horizon 2020 research and innovation program grant agreement 714936 (ERC–STG TRUE DEPTHS) to M. Alvaro. Alvaro and Scambelluri acknowledge the Ministero dell'Istruzione dell'Università e della Ricerca (MIUR) Progetti di Ricerca di Interesse Nazionale (PRIN) Bando PRIN 2017—Prot. 2017ZE49E7_005 for funding. We thank the two anonymous reviewers and the Editor Katy Evans for their comments and suggestions which helped improving the first version of this manuscript. We also thank A. Risplendente for technical assistance during the EMPA work.

## ORCID

*Mattia Gilio* https://orcid.org/0000-0002-7299-3377

## REFERENCES

Ague, J. J., & Eckert, J. O. Jr (2012). Precipitation of rutile and ilmenite needles in garnet: Implications for extreme metamorphic conditions in the Acadian Orogen, USA. *American Mineralogist*, *97*(5–6), 840–855. https://doi.org/10.2138/am.2012.4015

Alvaro, M., Mazzucchelli, M. L., Angel, R. J., Murri, M., Campomenosi, N., Scambelluri, M., Nestola, F., Korsakov, A., Tomilenko, A. A., Marone, F., & Morana, M. (2020). Fossil subduction recorded by quartz from the coesite stability field. *Geology*, *48*(1), 24–28. https://doi.org/10.1130/G46617.1

Angel, R. J., Alvaro, M., Miletich, R., & Nestola, F. (2017). A simple and generalised P-T–V EoS for continuous phase transitions, implemented in EosFit and applied to quartz. *Contributions to Mineralogy and Petrology*, *172*(5), 29. https://doi.org/10.1007/s00410-017-1349-x

Angel, R. J., Mazzucchelli, M. L., Alvaro, M., & Nestola, F. (2017). EosFit-Pinc: A simple GUI for host-inclusion elastic thermobarometry. *American Mineralogist*, *102*(9), 1957–1960. https://doi.org/10.2138/am-2017-6190

Angel, R. J., Mazzucchelli, M. L., Alvaro, M., Nimis, P., & Nestola, F. (2014). Geobarometry from host-inclusion systems: The role of elastic relaxation. *American Mineralogist*, *99*(10), 2146–2149. https://doi.org/10.2138/am-2014-5047

Angel, R. J., Murri, M., Mihailova, B., & Alvaro, M. (2019). Stress, strain and Raman shifts. *Zeitschrift Für Kristallographie-Crystalline Materials*, *234*(2), 129–140. https://doi.org/10.1515/zkri-2018-2112

Binvignat, F. A. P., Malcherek, T., Angel, R. J., Paulmann, C., Schlüter, J., & Mihailova, B. (2018). Radiation-damaged zircon under high pressures. *Physics and Chemistry of Minerals*, *45*(10), 981–993. https://doi.org/10.1007/s00269-018-0978-6

Campomenosi, N., Mazzucchelli, M. L., Mihailova, B., Scambelluri, M., Angel, R. J., & Alvaro, M. (2018). Elastic geobarometry: A comparison between experiments and numerical simulations. Paper presented at the EGU General Assembly Conference Abstracts.

Campomenosi, N., Rubatto, D., Hermann, J., Mihailova, B., Scambelluri, M., & Alvaro, M. (2020). Establishing a protocol for the selection of zircon inclusions in garnet for Raman thermobarometry. *American Mineralogist*, *105*, 992–1001. https://doi.org/10.2138/am-2020-7246

Campomenosi, N., Scambelluri, M., Angel, R. J., Hermann, J., Mazzucchelli, M. L., Mihailova, B., Piccoli, F., & Alvaro, M. (2021). Using the elastic properties of zircon-garnet host-inclusion pairs for thermobarometry of the ultrahigh-pressure Dora-Maira whiteschists: Problems and perspectives. *Contributions to Mineralogy and Petrology*, *176*(5), 1–17. https://doi.org/10.1007/s00410-021-01793-6

Carswell, D. A., & Van Roermund, H. L. (2005). On multi-phase mineral inclusions associated with microdiamond formation in mantle-derived peridotite lens at Bardane on Fjørtoft, west Norway. *European Journal of Mineralogy*, *17*(1), 31–42.

Carswell, D., Van Roermund, H., & de Vries, D. W. (2006). Scandian ultrahigh-pressure metamorphism of Proterozoic basement rocks on Fjørtoft and Otrøy, Western Gneiss Region, Norway. *International Geology Review*, *48*(11), 957–977. https://doi.org/10.2747/0020-6814.48.11.957

Cesare, B., Parisatto, M., Mancini, L., Peruzzo, L., Franceschi, M., Tacchetto, T., & Marone, F. (2020). Mineral inclusions are not immutable: Evidence of post-entrapment thermally-induced shape change of quartz in garnet. *Earth and Planetary Science Letters*, *555*, 116708.

Connolly, J. (1990). Multivariable phase diagrams: An algorithm based on generalized thermodynamics. *American Journal of Science*, *290*, 666–718. https://doi.org/10.2475/ajs.290.6.666

Corfu, F., Andersen, T., & Gasser, D. (2014). The Scandinavian Caledonides: Main features, conceptual advances and critical questions. *Geological Society, London, Special Publications*, *390*(1), 9–43. https://doi.org/10.1144/SP390.25

Cuthbert, S., Carswell, D., Krogh-Ravna, E., & Wain, A. (2000). Eclogites and eclogites in the Western Gneiss region, Norwegian Caledonides. *Lithos*, *52*(1–4), 165–195. https://doi.org/10.1016/S0024-4937(99)00090-0

Dobrzhinetskaya, L. F., Eide, E. A., Larsen, R. B., Sturt, B. A., Trønnes, R. G., Smith, D. C., Taylor, W. R., & Posukhova, T. V. (1995). Microdiamond in high-grade metamorphic rocks of the Western Gneiss region, Norway. *Geology*, *23*(7), 597–600. https://doi.org/10.1130/0091-7613(1995)023<0597:MIHGMR>2.3.CO;2

Ehlers, A. M., Zaffiro, G., Angel, R. J., Boffa-Ballaran, T., Carpenter, M., Alvaro, M., & Ross, N. L. (in press). Thermoelastic properties of zircon: Implications for geothermobarometry. *American Mineralogist*. https://doi.org/10.2138/am-2021-7731

Gilio, M., Angel, R. J., & Alvaro, M. (in press). Elastic geobarometry: How to work with residual inclusion strains and pressures. *American Mineralogist*. https://doi.org/10.2138/am-2021-7928

Gorbatschev, R. (1985). Precambrian basement of the Scandinavian Caledonides. In D. G. Gee, B. A. Sturt (Eds.), *The Caledonide Orogen—Scandinavia and related areas* (vol. 197, p. 212). Wiley.

Holland, T., & Powell, R. (2011). An improved and extended internally consistent thermodynamic dataset for phases of petrological interest, involving a new equation of state for solids. *Journal of Metamorphic Geology*, *29*(3), 333–383. https://doi.org/10.1111/j.1525-1314.2010.00923.x

Kohn, M. J. (2014). "Thermoba-Raman-try": Calibration of spectroscopic barometers and thermometers for mineral inclusions. *Earth and Planetary Science Letters*, *388*, 187–196. https://doi.org/10.1016/j.epsl.2013.11.054

Kohn, M. J. (2020). A refined zirconium-in-rutile thermometer. *American Mineralogist: Journal of Earth and Planetary Materials*, *105*(6), 963–971. https://doi.org/10.2138/am-2020-7091

Krogh Ravna, E., & Terry, M. P. (2004). Geothermobarometry of UHP and HP eclogites and schists–An evaluation of equilibria among garnet–clinopyroxene–kyanite–phengite–coesite/quartz. *Journal of Metamorphic Geology*, *22*(6), 579–592. https://doi.org/10.1111/j.1525-1314.2004.00534.x

Kuzmany, H. (2009). Light scattering spectroscopy. *Solid-state spectroscopy* (pp. 183–215). Springer.

Larsen, R. B., Eide, E. A., & Burke, E. A. (1998). Evolution of metamorphic volatiles during exhumation of microdiamond-bearing granulites in the Western Gneiss Region, Norway. *Contributions to Mineralogy and Petrology*, *133*(1–2), 106–121. https://doi.org/10.1007/s004100050441

Liu, P., & Massonne, H. J. (2019). An anticlockwise P-T-t path at high-pressure, high-temperature conditions for a migmatitic gneiss from the island of Fjørtoft, Western Gneiss Region, Norway, indicates two burial events during the Caledonian orogeny. *Journal of Metamorphic Geology*, *37*(4), 567–588.

Mazzucchelli, M. L., Angel, R. J., & Alvaro, M. (2021). EntraPT: An online platform for elastic geothermobarometry. *American Mineralogist*, *106*(5), 830–837. https://doi.org/10.2138/am-2021-7693CCBYNCND

Mazzucchelli, M., Burnley, P., Angel, R., Morganti, S., Domeneghetti, M., Nestola, F., & Alvaro, M. (2018). Elastic geothermobarometry: Corrections for the geometry of the host-inclusion system. *Geology*, *46*(3), 231–234. https://doi.org/10.1130/G39807.1

Mazzucchelli, M. L., Reali, A., Morganti, S., Angel, R., & Alvaro, M. (2019). Elastic geobarometry for anisotropic inclusions in cubic hosts. *Lithos*, *350*, 105218. https://doi.org/10.1016/j.lithos.2019.105218

Milani, S., Nestola, F., Alvaro, M., Pasqual, D., Mazzucchelli, M., Domeneghetti, M., & Geiger, C. (2015). Diamond–garnet geobarometry: The role of garnet compressibility and expansivity. *Lithos*, *227*, 140–147. https://doi.org/10.1016/j.lithos.2015.03.017

Mørk, M. B. E. (1985). A gabbro to eclogite transition on Flemsøy, Sunnmøre, western Norway. *Chemical Geology*, *50*(1–3), 283–310. https://doi.org/10.1016/0009-2541(85)90125-1

Murri, M., Mazzucchelli, M. L., Campomenosi, N., Korsakov, A. V., Prencipe, M., Mihailova, B. D., & Alvaro, M. (2018). Raman elastic geobarometry for anisotropic mineral inclusions. *American Mineralogist*, *103*(11), 1869–1872.

Özkan, H., Cartz, L., & Jamieson, J. (1974). Elastic constants of nonmetamict zirconium silicate. *Journal of Applied Physics*, *45*(2), 556–562. https://doi.org/10.1063/1.1663283

Powell, R., Holland, T., & Worley, B. (1998). Calculating phase diagrams involving solid solutions via non-linear equations, with examples using THERMOCALC. *Journal of Metamorphic Geology*, *16*(4), 577–588. https://doi.org/10.1111/j.1525-1314.1998.00157.x

Robinson, P., Terry, M. P., Carswell, D., Van Roermund, H., Krogh, T. E., Root, D., & Solli, A. (2003). Tectono-stratigraphic setting, structure and petrology of HP and UHP metamorphic rocks and garnet peridotites in the Western Gneiss Region, Møre og Romsdal, Norway. Norges geologiske undersøkelse, Report.

Rosenfeld, J. L., & Chase, A. B. (1961). Pressure and temperature of crystallization from elastic effects around solid inclusions in minerals? *American Journal of Science*, *259*(7), 519–541. https://doi.org/10.2475/ajs.259.7.519

Scambelluri, M., Pettke, T., & Van Roermund, H. (2008). Majoritic garnets monitor deep subduction fluid flow and mantle dynamics. *Geology*, *36*(1), 59–62. https://doi.org/10.1130/G24056A.1

Scambelluri, M., Van Roermund, H. L., & Pettke, T. (2010). Mantle wedge peridotites: Fossil reservoirs of deep subduction zone processes: Inferences from high and ultrahigh-pressure rocks from Bardane (Western Norway) and Ulten (Italian Alps). *Lithos*, *120*(1), 186–201. https://doi.org/10.1016/j.lithos.2010.03.001

Stangarone, C., Angel, R. J., Prencipe, M., Campomenosi, N., Mihailova, B., & Alvaro, M. (2019). Measurement of strains in zircon inclusions by Raman spectroscopy. *European Journal of Mineralogy*, *31*(4), 685–694. https://doi.org/10.1127/ejm/2019/0031-2851

Stern, R. J. (2002). Subduction zones. *Reviews of Geophysics*, *40*(4), 3-1-3-38. https://doi.org/10.1029/2001RG000108

Tajčmanová, L., Manzotti, P., & Alvaro, M. (2021). Under pressure: High-pressure metamorphism in the Alps. *Elements: An International Magazine of Mineralogy, Geochemistry, and Petrology*, *17*(1), 17–22. https://doi.org/10.2138/gselements.17.1.17

Terry, M. P., & Robinson, P. (2003). Evolution of amphibolite-facies structural features and boundary conditions for deformation during exhumation of high-and ultrahigh-pressure rocks, Nordøyane, Western Gneiss Region, Norway. *Tectonics*, *22*(4). https://doi.org/10.1029/2001TC001349

Terry, M. P., Robinson, P., & Ravna, E. J. K. (2000). Kyanite eclogite thermobarometry and evidence for thrusting of UHP over HP metamorphic rocks, Nordøyane, Western Gneiss Region, Norway. *American Mineralogist*, *85*(11–12), 1637–1650. https://doi.org/10.2138/am-2000-11-1207

Thomas, J. B., & Spear, F. S. (2018). Experimental study of quartz inclusions in garnet at pressures up to 3.0 GPa: Evaluating validity of the quartz-in-garnet inclusion elastic thermobarometer. *Contributions to Mineralogy and Petrology*, *173*, 1–14.

Thomas, J. B., Watson, E. B., Spear, F. S., Shemella, P. T., Nayak, S. K., & Lanzirotti, A. (2010). TitaniQ under pressure: The effect of pressure and temperature on the solubility of Ti in quartz. *Contributions to Mineralogy and Petrology*, *160*(5), 743–759. https://doi.org/10.1007/s00410-010-0505-3

Tomkins, H., Powell, R., & Ellis, D. (2007). The pressure dependence of the zirconium-in-rutile thermometer. *Journal of Metamorphic Geology*, *25*(6), 703–713. https://doi.org/10.1111/j.1525-1314.2007.00724.x

van Roermund, H. L. (2009). Mantle-wedge garnet peridotites from the northernmost ultra-high pressure domain of the Western Gneiss Region, SW Norway. *European Journal of Mineralogy*, *21*(6), 1085–1096. https://doi.org/10.1127/0935-1221/2009/0021-1976

van Roermund, H. L., Carswell, D. A., Drury, M. R., & Heijboer, T. C. (2002). Microdiamonds in a megacrystic garnet websterite pod from Bardane on the island of Fjørtoft, western Norway: Evidence for diamond formation in mantle rocks during deep continental subduction. *Geology*, *30*(11), 959–962. https://doi.org/10.1130/0091-7613(2002)030<0959:MIAMGW>2.0.CO;2

van Roermund, H. L., & Drury, M. R. (1998). Ultra-high pressure (P> 6 GPa) garnet peridotites in Western Norway: Exhumation of mantle rocks from> 185 km depth. *Terra Nova*, *10*(6), 295–301.

Vrijmoed, J. C., Podladchikov, Y. Y., Andersen, T. B., & Hartz, E. H. (2009). An alternative model for ultra-high pressure in the Svartberget Fe-Ti garnet-peridotite, Western Gneiss Region, Norway. *European Journal of Mineralogy*, *21*(6), 1119–1133. https://doi.org/10.1127/0935-1221/2009/0021-1985

Vrijmoed, J., Van Roermund, H., & Davies, G. (2006). Evidence for diamond-grade ultra-high pressure metamorphism and fluid interaction in the Svartberget Fe–Ti garnet peridotite–websterite body, Western Gneiss Region, Norway. *Mineralogy and Petrology*, *88*(1–2), 381–405. https://doi.org/10.1007/s00710-006-0160-6

Walczak, K., Cuthbert, S., Kooijman, E., Majka, J., & Smit, M. A. (2019). U-Pb zircon age dating of diamond-bearing gneiss from Fjørtoft reveals repeated burial of the Baltoscandian margin during the Caledonian Orogeny. *Geological Magazine*, *156*(11), 1–16. https://doi.org/10.1017/S0016756819000268

Wang, J., Mao, Z., Jiang, F., & Duffy, T. S. (2015). Elasticity of single-crystal quartz to 10 GPa. *Physics and Chemistry of Minerals*, *42*(3), 203–212.

Watson, E., Wark, D., & Thomas, J. (2006). Crystallization thermometers for zircon and rutile. *Contributions to Mineralogy and Petrology*, *151*(4), 413. https://doi.org/10.1007/s00410-006-0068-5

Zhang, Y. (1998). Mechanical and phase equilibria in inclusion–host systems. *Earth and Planetary Science Letters*, *157*(3–4), 209–222. https://doi.org/10.1016/S0012-821X(98)00036-3

Zheng, Y.-F., & Hermann, J. (2014). Geochemistry of continental subduction-zone fluids. *Earth, Planets and Space*, *66*(1), 93. https://doi.org/10.1186/1880-5981-66-93

## SUPPORTING INFORMATION

Additional supporting information may be found online in the Supporting Information section.

**Figure S1**. Microphotographs of inclusions in garnet from the samples FJ1702 (a–d) and FJ1704 (e–h)

**Figure S2**. Raman spectra of sillimanite (black), kyanite (blue) and host garnet (orange)

**Table S1**. EMP analyses of garnets

**Table S2**. Raman peak positions, Δω, strain and stress of analyzed quartz and zircon inclusions

**Table S3**. Raman peak positions of free (unstrained) quartz and zircon reference crystals

**How to cite this article:** Gilio, M., Scambelluri, M., Angel, R. J., & Alvaro, M. (2022). The contribution of elastic geothermobarometry to the debate on HP versus UHP metamorphism. *Journal of Metamorphic Geology, 40*(2), 229–242. https://doi.org/10.1111/jmg.12625